Proc. Natl. Acad. Sci. USA
Vol. 77, No. 8, pp. 4633–4637, August 1980
Biochemistry

Structure of the potato inhibitor complex of carboxypeptidase A at 2.5-Å resolution

(enzyme complex/protease inhibitor/protein crystallography)

DOUGLAS C. REES AND WILLIAM N. LIPSCOMB*

Gibbs Chemical Laboratory, Harvard University, Cambridge, Massachusetts 02138

Contributed by William N. Lipscomb, May 16, 1980

ABSTRACT **The structure of the complex between the proteolytic enzyme carboxypeptidase A (peptidyl-L-amino-acid hydrolase, EC 3.4.17.1) and the 39-amino-acid carboxypeptidase A inhibitor from potatoes has been determined at 2.5-Å resolution. A combination of multiple isomorphous replacement, molecular replacement, and noncrystallographic symmetry averaging techniques was used to solve the structure. The chain trace of the inhibitor and details of the binding interactions in the complex are described. A surprising aspect of the complex is that the carboxy-terminal peptide bond of the inhibitor has been hydrolyzed, and the carboxy-terminal glycine is trapped in the binding pocket of carboxypeptidase A. Consequently, the complex resembles a stage in the catalytic mechanism after hydrolysis of the peptide bond. The ring of tyrosine-248, which is known to undergo large conformational changes upon substrate binding, is in the "down" position and interacts with the inhibitor in the complex.**

Significant changes in the conformation of residues near the active site of carboxypeptidase A (CPase A; peptidyl-L-amino-acid hydrolase, EC 3.4.17.1) accompany the binding of substrates to this enzyme (1). In the most dramatic instance, the hydroxyl of Tyr-248 shifts 12 Å from the native position upon binding of the dipeptide Gly-Tyr (1), or binding of the ester analogue (−)-2-benzyl-3-*p*-methoxybenzoylpropionate (2). Biochemical methods have also demonstrated that substrate–enzyme interactions in CPase A may influence the behavior of residues over 15 Å from the active site. Abramowitz *et al.* (3) observed that at least five carboxy-terminal residues of the substrate may influence both the binding and the catalytic parameters of hydrolysis. The structural details responsible for the transmission of binding information to the active site, however, have yet to be established.

We have undertaken a crystallographic study of the complex between CPase A and the 39-amino-acid carboxypeptidase inhibitor from potatoes (PCI) in an effort to determine how extended substrates bind to CPase A and how these binding interactions may influence the catalytic mechanism (4). The sequence and disulfide pairings of PCI (5, 6) are illustrated in Fig. 1. In addition, the structure of another crystal form of CPase A should be of great relevance in resolving the controversy concerning the integrity of the molecular structure in solution as compared with the structure in the various crystalline phases. In particular, the conclusions of the x-ray diffraction studies of CPase A have been questioned (7, 8) on the basis of the low reactivity (1/300) towards small substrates of one crystalline phase, even though the x-ray diffraction studies were made on a different crystal form that has an activity of about

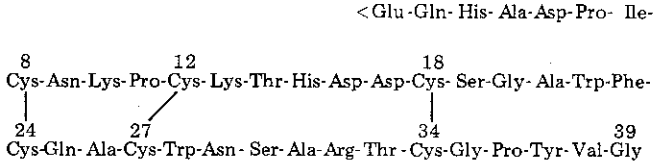

FIG. 1. Amino acid sequence of PCI.

1/3 of that in solution (9, 10). This paper reports the structure at 2.5-Å resolution of the CPase A–PCI structure and presents a preliminary interpretation of the binding interactions in the complex.

METHODS

As previously described (4), crystals of the CPase A–PCI complex (space group $P3_2$, a = 53.45 Å, c = 218.5 Å), grown by vapor diffusion against polyethylene glycol, exhibited twinning by merohedry, with an average twinning fraction of 0.35. The complex was dissolved in 0.2 M LiCl/0.01 M Tris·HCl, pH 7.5/4% (vol/vol) polyethylene glycol-6000. Dialysis of this solution against 0.12 M LiCl/0.01 M Tris·HCl, pH 7.5/4% (vol/vol) polyethylene glycol-6000, at 4°C yielded crystals in the same space group, but with a lower mean twinning fraction (≈0.15). Consequently, crystals grown by dialysis were used for the high-resolution data collection.

Full data sets were collected from single crystals by using the oscillation film method. The x-ray source was an Elliot GX-3, focused by a Franks double-mirror system (11). Crystals were mounted with the c axis along the oscillation camera axis. Complete data sets required 20 3° oscillation films, with 3.5 hr of exposure per film. Film scanning and data processing procedures are described in ref 12.

Conditions for the preparation of heavy atom derivatives differed slightly from those used in the low-resolution work (4) and are listed in Table 1. Because the degree of twinning in each crystal could not be estimated optically, in general several crystals for each soak were collected, and the data set with the lowest twinning fraction (as estimated by visual inspection of pseudosymmetry in the *hhl* zone) was processed. Data sets for the native protein and for the $HgCl_2$, $AgNO_3$, and K_2PtCl_4 derivatives were collected to 2.5-Å resolution, and data for the $K_2Pt(NO_2)_4$ derivative to 2.8-Å resolution. Values of $R = \Sigma|I_i - I_j|/\Sigma|I_i + I_j|$, summed over all symmetry-related reflections i and j, were 0.074, 0.089, 0.077, 0.082, and 0.057 for the

The publication costs of this article were defrayed in part by page charge payment. This article must therefore be hereby marked "*advertisement*" in accordance with 18 U. S. C. §1734 solely to indicate this fact.

Abbreviations: CPase A, carboxypeptidase A; PCI, potato carboxypeptidase inhibitor; MIR, multiple isomorphous replacement; MR, molecular replacement.

* To whom reprint requests should be addressed.

Table 1. Preparation of heavy atom derivatives

Compound	Conc., mM	Soaking time, days	Buffer*
$HgCl_2$	2	24	LiCl/Tris
$AgNO_3$	3	9	Acetate
$K_2Pt(NO_2)_4$	2	5	LiCl/Tris
K_2PtCl_4	3	9	LiCl/Tris

* LiCl/Tris, 0.12 M LiCl/0.01 M Tris·HCl, pH 7.5/4% polyethylene glycol-6000; acetate, 0.05 M NaCl/0.02 M Tris·acetic acid, pH 7.5/4% polyethylene glycol-6000.

native, $HgCl_2$, $AgNO_3$, K_2PtCl_4, and $K_2Pt(NO_2)_4$ data sets, respectively.

Twinning fractions of the data sets were estimated by using tests based on intensity statistics (13) and tests based on correlations between the intensities of twin related reflections (14, 15). The results of each method agreed to within a few percent, and they established twinning fractions of 0.10, 0.15, 0.30, 0.14, and 0.42 for the native, $HgCl_2$, $AgNO_3$, K_2PtCl_4, and $K_2Pt(NO_2)_4$ data sets, respectively. Because of the relatively small twinning fractions of the native, $HgCl_2$ and K_2PtCl_4 data sets, and the relatively large errors associated with twinning corrections (16), it was decided to neglect twinning corrections at this stage of the study.

Location and Refinement of Heavy Atom Parameters. Heavy atom difference Patterson maps of the $HgCl_2$ and $K_2Pt(NO_2)_4$ derivatives were cleanly interpretable and provided the initial heavy atom positions for phase refinement. Heavy atom sites in the $AgNO_3$ and K_2PtCl_4 derivatives were located by using these phases. Initial heavy atom positions, occupancies, and temperature factors were refined by using cycles of multiple isomorphous replacement (MIR) centroid phasing and least squares (17). The presence of additional sites and the validity of old sites were determined by using residual difference Fourier syntheses (18). The final heavy atom parameters, which were refined in space group $P3_1$ for historical reasons, appear in Table 2. The overall figure of merit at 2.5-Å resolution was 0.56, with 93% of the total possible structure factors phased. Phasing statistics for the last refinement cycle are given in Table 3. The variations in figure of merit and phasing power of each derivative with resolution are illustrated in Fig. 2.

Table 2. Heavy atom parameters

Site	Occupancy	Axes x	y	z	B, Å^{-2} *
$HgCl_2$					
1	0.31	0.403	0.888	0.0593	19.97
2	0.52	0.481	0.907	0.0370	31.96
3	0.47	0.935	0.452	−0.0335	8.01
4	0.30	0.913	0.371	−0.0559	13.34
$AgNO_3$					
1	0.41	0.932	0.905	−0.0010	13.80
2	0.56	0.490	0.908	0.0348	26.05
3	0.13	−0.003	0.301	0.0745	18.42
4	0.63	0.805	0.446	0.1095	9.55
5	0.46	0.335	0.173	0.1295	16.55
6	0.46	0.198	0.300	−0.1289	20.20
7	0.49	0.450	0.749	−0.1104	11.39
8	0.61	0.942	0.459	−0.0363	13.71
$K_2Pt(NO_2)_4$					
1	0.77	0.806	0.444	0.1100	25.43
2	0.47	0.450	0.758	−0.1094	14.54
K_2PtCl_4					
1	0.13	0.628	0.789	0.0030	1.66
2	0.19	0.327	−0.009	0.0655	28.20
3	0.13	0.674	0.171	0.1064	3.15
4	0.22	0.806	0.439	0.1115	21.25
5	0.20	0.447	0.768	−0.1070	0.53
6	0.15	0.196	0.648	−0.1023	28.44
7	0.22	0.013	0.291	−0.0638	14.65

* B, isotropic temperature factor.

Table 3. Statistics of MIR phasing at 2.5-Å resolution*

Derivative	rms f_c†	rms e_j‡	R_K§
$HgCl_2$	72.8	44.0	0.116
$AgNO_3$	73.6	54.3	0.151
$K_2Pt(NO_2)_4$	75.4	60.5	0.107
K_2PtCl_4	45.5	48.6	0.134

* The overall figure of merit was 0.56.

† rms, Root mean square. rms $f_c = (\Sigma f_{hj}^2/n)^{1/2}$, in which f_{hj} is the heavy atom scattering amplitude for reflection h of derivative j. The rms structure factor of the native protein was 260.

‡ rms $e_j = (\Sigma e_{hj}^2/n)^{1/2}$, in which e_{hj} is the lack of closure for reflection h of derivative j.

§ $R_K = \Sigma(\|F_{pH}^o| - |F_p^c + f_h\|)/\Sigma(F_{pH}^o)$ summed over all reflections, in which F_{pH}^o is the absolute observed structure factor for the derivative and F_p^c and f_h are the calculated structure factors for the native protein and heavy atom, respectively.

Phase Refinement. A 2.5-Å resolution map was calculated with figure of merit weighted centroid MIR phases (19). The highest electron density in this map was at the zinc site, and α helices and β strands of the native enzyme were clearly visible. Strong density was also present in the active site pocket. Connectivity of the peptide chain was not always satisfactory, however, so that the map was averaged about the noncrystallographic symmetry axis in an attempt to improve it. The location of the noncrystallographic symmetry axis was refined

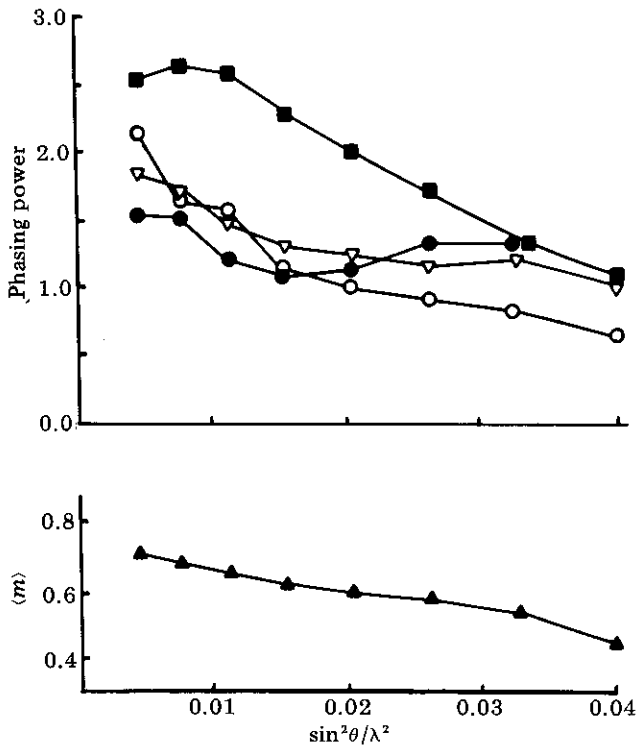

FIG. 2. Variation in figure of merit ($\langle m \rangle$) and phasing power ($= \langle f_c \rangle / \langle e_j \rangle$) with resolution. Phasing power for $HgCl_2$ (■), $AgNO_3$ (▽), $K_2Pt(NO_2)_4$ (●), and K_2PtCl_4 (○) is shown.

from the MIR electron density map by using the method of Cox (20). The spherical angles relating the rotation of one molecule to another were $\phi = 0.5°$, $\theta = 59.8°$, $\kappa = 179.9°$ [notation of Rossmann and Blow (21)], with a translation component of $x = -1.35$ Å, $y = 2.05$ Å, and $z = -0.45$ Å. If the noncrystallographic symmetry axis were a crystallographic twofold axis, the corresponding parameters would be $\phi = 0.0°$, $\theta = 60.0°$, $\kappa = 180.0°$, $x = y = z = 0.0$ Å. Consequently, the noncrystallographic symmetry axis has nearly the same direction as a crystallographic twofold axis would have but is translationally displaced from that orientation. The averaging of the map was performed by using a system of programs developed by Bricogne (22).

Although the map was improved by averaging and many features of the native structure could be discerned, connectivity of the peptide chain was still poor in some regions of the map. Consequently, it was decided to incorporate phase information from the native structure into the MIR phases and refine the combined phases by exploiting the noncrystallographic symmetry of the complex. The theory and early applications of these molecular replacement (MR) and real space averaging methods have been described by Rossmann (23).

Initial MR parameters for placing the native CPase A coordinates in the CPase A–PCI unit cell were estimated from the positions of heavy atom sites common to the native and CPase A–PCI structures. These parameters were then refined by a least squares minimization of the residual $(|F_o| - |F_c|)^2$, in which F_o and F_c are the observed and calculated structure factors, respectively, as a function of the appropriate rigid body rotation and translation parameters. By using fast Fourier structure factor programs written by ten Eyck (24), 2.5-Å resolution structure factors were calculated with the refined MR parameters. To avoid biasing the phases, all residues in the active site of CPase A were omitted from the structure factor calculation. The R-factor between calculated and observed structure factors was 0.42 at 2.5-Å resolution, with an average phase shift between MR and MIR phases of 75.9°. On the basis of figure of merit, a phase error of 56° is expected in the MIR phases alone. The MIR and MR phase sets were then combined by using a modified Sims formula (22). The combined and MIR phase sets differed by 30.4°.

Starting with this combined phase set, three cycles of phase refinement using Bricogne's real space phase refinement method were initiated (22). The envelope surrounding the complex was prepared on an Evans and Sutherland tablet, using a program written by C. Steele and P. Kuttner. The statistics of phase refinement (Table 4) indicated that convergence had been achieved after three cycles. Examination of electron density maps at various stages of refinement indicated that connectivity in both the native and inhibitor regions of the electron density map had been improved by this procedure.

Table 4. Statistics of real space phase refinement

Phase set	$\langle\|\Delta\Phi\|\rangle$,* degrees	R†
Combined vs. cycle 1	34.5	0.29
Cycle 2 vs. cycle 1	9.3	0.19
Cycle 3 vs. cycle 2	5.7	0.17
MIR vs. cycle 3	41.0	

* $\langle|\Delta\Phi|\rangle$ = average absolute phase difference between phase sets.
† $R = \Sigma|F_o - F_c|/\Sigma|F_o|$, in which F_o is the observed structure factor and F_c is the structure factor calculated from a symmetrized electron density map.

RESULTS AND DISCUSSION

The final electron density map clearly shows that the carboxy terminus of PCI is bound to the active site of CPase A. Starting from this site, it is possible to trace the entire path of the inhibitor peptide chain (Fig. 3). With one important exception (discussed below), there are only two gaps in the chain, between residues 14–15 and 33–34. (Given the region of interaction of PCI with CPase A, all residues with sequence numbers less than 40 will refer to PCI residues.) In both cases, correlation of structural and sequence information confirms the crossing of the gaps. In addition, there is very poor density for residues Ser-19-Ala-21, and the first three residues of PCI cannot be unambiguously located. These regions of PCI are in near contact with the noncrystallographically related CPase A molecule, and it is possible that residues in this area do not strictly obey the noncrystallographic symmetry. The averaging procedure employed for phase refinement would consequently tend to "washout" the density in such regions.

PCI has no helices or sheets, although residues 25–29 are in an extended conformation. One of the striking features of the structure is that the disulfide bond between Cys-18 and Cys-34 passes through a loop generated by the other two disulfide bonds. This knot distinguishes the domain structure of wheat germ agglutinin (25) from PCI, even though these two proteins have the same pattern of cysteine pairings. The number of residues between cysteines differs for the two proteins, however, thus permitting different topological arrangements of the peptide chain to occur.

The PCI peptide chain may be traced towards the active site of CPase A to Val-38, the carboxy terminus of which is bound to the zinc. A distinct gap, approximately 4 Å long, exists be-

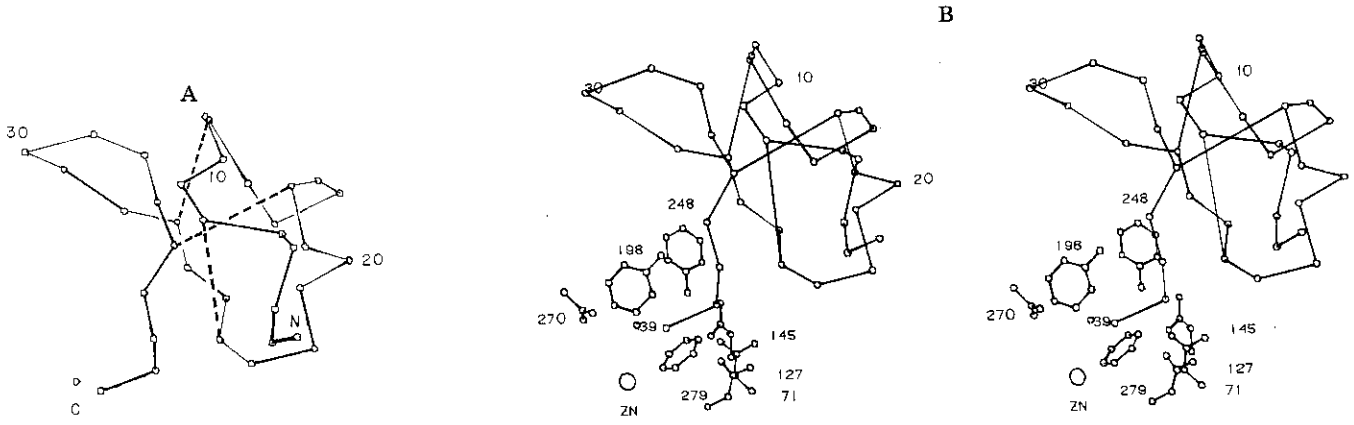

FIG. 3. Structure of PCI. View is down the z axis, with the $(11\bar{2}0)$ axis vertical. (A) Chain trace of α carbons (residues 3–39) and disulfide bonding of PCI. N and C, amino and carboxy termini. (B) Stereoview of PCI with associated active site side chains of CPase A.

tween the densities for Val-38 and Gly-39, however. Density presumably attributable to Gly-39 not only is present where the carboxyl group of the Gly-Tyr dipeptide was located (1) but also extends past this position into the active site pocket. As a result, the overall impression is that the gap between Val-38 and Gly-39 has been caused by the hydrolysis and subsequent entrapment of Gly-39 in the active site pocket, and not just partial obliteration of the Val-38—Gly-39 peptide bond. The latter effect could be produced by rippling of the electron density around the zinc due to imperfect phasing (26). The density, however, is of the appropriate size for a glycine molecule—too large for a water molecule, and too small for a Tris molecule from the buffer.

The binding interactions of CPase A and PCI are generally consistent with the binding mode for extended substrates to CPA proposed by Lipscomb *et al.* (1). Of special interest, the Tyr-248 ring is in the "down" position and appears to interact with both the Tyr-37—Val-38 peptide bond and the Val-38 carboxylate–zinc complex. Glu-270 is directed towards the Val-38 carboxyl group, although Glu-270 side-chain density does not extend completely to the valine, implying that an anhydride linkage is not present in this complex. PCI is oriented in such a manner that it can interact with all three arginines (145, 127, and 71) that extend along the active site binding groove of CPase A. The carboxylate group of Gly-39 binds to Arg-145, Arg-127 is near both the Val-38 carboxylate group and the carbonyl of the Tyr-37—Val-38 peptide bond, and Arg-71 is suitably positioned to interact with the Tyr-37—Val-38 peptide bond. The ring of Tyr-37 is directed between the side chains of Thr-164 and Tyr-248 of CPase A. Residues Tyr-198 and Phe-279, proposed as one of the principal binding regions for extended substrates, cover the peptide backbone around Tyr-37.

Because of the sharp turn in the peptide chain due to Pro-36, only residues 37–39 of PCI interact appreciably with the active site of CPase A. Consequently, only three of the five subsites proposed by Abramowitz *et al.* (3) are occupied in this complex. Interactions between other regions of PCI and CPase A occur, however, which must be responsible for the much tighter binding of PCI to CPase A than that of normal peptide substrates. The peptide chain of Trp-28—Ser-30 binds near the backbone of residues Ile-247—Tyr-248 and the side chain of Lys-239. The side chain of Trp-28 interacts extensively with Leu-202 and the backbone of Tyr-198 and Ser-199, while the phenyl ring of Phe-21 is near the ring of Phe-279. There appears to be some contact between the side chain of His-15 and the ring of Tyr-248. Interestingly, the imidazole group of His-15 is located near the position that the Tyr-248 ring occupies in the native "up" position. Finally, in interactions that are probably of no physiological significance, the amino-terminal residues of PCI bind near Tyr-198 of the noncrystallographically related CPase A molecule, while Trp-22 interacts with the side chains of Phe-277 and Arg-276 of the adjacent CPase A molecule. Although the amino terminus of PCI passes near the Cys-8—Cys-24 disulfide bond of the noncrystallographically related PCI molecule, there appear to be no extensive dimer contacts between these PCI molecules.

Consistent with the CPase A–PCI complex structure, chemical modification studies on PCI had predicted the involvement of Gly-39 and Tyr-37 and a smaller role for His-15 in inhibitor binding to CPase A (27). Likewise, the crystal structure confirms the lack of involvement of Lys, Arg, and Asp side chains, and the amino-terminal five amino acids, in the binding to CPase A. On the basis of the structure of the complex, however, both Trp residues would be expected to be substantially exposed to solvent in free PCI, which contradicts the conclusions drawn from the lack of reactivity of these residues with modifying reagents.

The CPase A–PCI complex appears to represent a stage in catalysis after hydrolysis of the peptide bond. This is very different from x-ray diffraction structures of complexes of serine proteases with protein protease inhibitors. Here, the carbonyl carbon of the reactive-site peptide bond of the inhibitor has a slight tendency towards tetrahedral geometry, indicative of a stage of catalysis prior to hydrolysis (28). Although serine proteases can hydrolyze the reactive-site peptide bond of the appropriate inhibitor, the two resulting peptide chains are held together by disulfide bonds, so that the modified species still retains inhibitory activity (29). In the CPase A–PCI complex, the reactive-site peptide bond is also hydrolyzed, but here Gly-39 is trapped in the active site pocket of CPAase A and cannot diffuse away. There is no evidence whether dissociation of PCI from CPase A requires resynthesis of the carboxy-terminal peptide bond or not. Also, there is presently no direct evidence as to whether PCI without Gly-39 is inactive as an inhibitor. If it were possible to generate des-Gly^{39}-PCI, then incubation of this protein with CPA in the presence of various free amino acids should generate modified species of PCI, differing in residue 39. An analogous reaction has been demonstrated for enzymatic replacement of reactive site residues in soybean trypsin inhibitor (30).

Refinement of the CPase A–PCI structure is essential to characterize structural details of the relationship between the zinc, Val-38, Gly-39, Glu-270, and Tyr-248, for possible clues pertaining to the hydrolytic mechanism. The binding of PCI to CPase A undoubtedly induces many subtle conformational changes in residues near the active site, which may influence catalysis. Once again, the most dramatic change is the large shift in orientation of the Tyr-248 ring. Model building and refinement of the electron density map will also permit a quantitative assessment of the variation in structure of CPase A between two unrelated crystal forms. Qualitative inspection of the MIR map of the CPase A–PCI complex, however, indicates that the gross conformation of the CPase A chain is very similar in the two structures. Consequently, it would appear that there is little reason to suspect significant differences between the molecular structure in solution as compared with that in several crystal structures (9, 10), although flexible side chains such as that of Tyr-248 and its region of attachment to the polypeptide backbone are particularly responsive to changes in pH and binding of substrates and inhibitors.

We thank the National Institutes of Health (Grant GM 06920) for support of this research. W.N.L. also thanks the Alexander von Humboldt Foundation for an award that aided this research.

1. Lipscomb, W., Hartsuck, J., Reeke, G., Quiocho, F., Bethge, P., Ludwig, M., Steitz, T., Muirhead, H. & Coppola, J. (1968) *Brookhaven Symp. Biol.* **21**, 24–90.
2. Rees, D. C., Honzatko, R. B. & Lipscomb, W. N. (1980) *Proc. Natl. Acad. Sci. USA* **77**, 3288–3291.
3. Abramowitz, N., Schechter, I. & Berger, A. (1967) *Biochem. Biophys. Res. Commun.* **29**, 862–867.
4. Rees, D. C. & Lipscomb, W. N. (1980) *Proc. Natl. Acad. Sci. USA* **77**, 277–280.
5. Hass, G., Nau, H., Biemann, K., Grahn, D., Ericsson, L. & Neurath, H. (1975) *Biochemistry* **14**, 1334–1342.
6. Leary, T., Grahn, D., Neurath, H. & Hass, G. (1979) *Biochemistry* **18**, 2252–2256.
7. Johansen, J. & Vallee, B. (1973) *Proc. Natl. Acad. Sci. USA* **70**, 2006–2010.
8. Spilburg, C., Bethune, J. & Vallee, B. (1977) *Biochemistry* **16**, 1142–1150.
9. Lipscomb, W. N. (1973) *Proc. Natl. Acad. Sci. USA* **70**, 3797–3801.

10. Lipscomb, W. N. (1980) *Proc. Natl. Acad. Sci. USA* **77**, 3875–3878.
11. Harrison, S. C. (1968) *J. Appl. Crystallogr.* **1**, 84–90.
12. Crawford, J. L. (1977) Dissertation (Harvard Univ., Cambridge, MA).
13. Rees, D. (1980) *Acta Crystallogr. Sect. A*, in press.
14. Murray-Rust, P. (1973) *Acta Crystallogr. Sect. B* **29**, 2559–2566.
15. Britton, D. (1972) *Acta Crystallogr. Sect. A* **28**, 296–297.
16. Grainger, C. (1969) *Acta Crystallogr. Sect. A* **25**, 427–434.
17. Dickerson, R., Kendrew, J. & Strandberg, B. (1961) *Acta Crystallogr.* **14**, 1188–1195.
18. Matthews, B. (1970) in *Crystallographic Computing*, eds. Ahmed, F., Hall, S. & Huber, C. (Munksgaard, Copenhagen), pp. 146–159.
19. Blow, D. & Crick, F. H. C. (1959) *Acta Crystallogr.* **12**, 794–802.
20. Cox, J. (1967) *J. Mol. Biol.* **28**, 151–156.
21. Rossmann, M. & Blow, D. (1963) *Acta Crystallogr.* **15**, 24–31.
22. Bricogne, G. (1976) *Acta Crystallogr. Sect. A* **32**, 832–847.
23. Rossmann, M., ed. (1972) *The Molecular Replacement Method* (Gordon & Breach, New York).
24. ten Eyck, L. (1977) *Acta Crystallogr. Sect. A* **33**, 486–492.
25. Wright, C. (1977) *J. Mol. Biol.* **111**, 439–457.
26. Buerger, M. (1960) *Crystal Structure Analysis* (Wiley, New York), pp. 596–600.
27. Hass, G., Ako, H., Grahn, D. & Neurath, H. (1976) *Biochemistry* **15**, 93–100.
28. Ruhlmann, A., Kukla, D., Schwager, P., Bartels, K. & Huber, R. (1973) *J. Mol. Biol.* **77**, 417–436.
29. Laskowski, M. & Sealock, R. (1972) in *The Enzymes*, ed. Boyer, P. (Academic, New York), Vol. 3, 3rd Ed., pp. 376–473.
30. Sealock, R. & Laskowski, M. (1969) *Biochemistry* **8**, 3703–3710.